



Downward current electron beam observed by Cluster and FAST

Andrew N. Wright,¹ Christopher J. Owen,² Christopher C. Chaston,³
and Malcolm W. Dunlop⁴

Received 16 July 2007; revised 30 October 2007; accepted 21 January 2008; published 3 June 2008.

[1] We report observations from a conjunction of FAST and Cluster during an interval of downward current at an MLT of 3–4 h on field lines mapping to the PSBL. Both spacecraft see upgoing electrons with an energy of a few hundred eV, suggesting substantial acceleration has occurred below FAST's altitude of 3200 km. At Cluster, isolated bursts of electrons are seen, and modeling indicates that the current mapped from the ionosphere exists as a collection of current filaments at Cluster (4–5 R_E). The current filaments are aligned with the background magnetic field and have a perpendicular scale at Cluster of about 100 km (which maps to 10–20 km in the ionosphere), and is similar to the mapped width observed by FAST. The electron beams are quasi-steady during a Cluster spacecraft transit time of 1 min. The field aligned current densities at FAST and Cluster are of the order of a few μAms^{-2} and $0.05 \mu\text{Am}^{-2}$, respectively, and j/B is conserved along a current filament.

Citation: Wright, A. N., C. J. Owen, C. C. Chaston, and M. W. Dunlop (2008), Downward current electron beam observed by Cluster and FAST, *J. Geophys. Res.*, 113, A06202, doi:10.1029/2007JA012643.

1. Introduction

[2] Downward current regions form an important part of the global magnetospheric current circuit. The downward current is carried predominantly by upward moving electrons of ionospheric origin [Marklund *et al.*, 1994; Carlson *et al.*, 1998a], and is associated with diverging electric fields. This field-aligned current is sometimes referred to as the return current and is often adjacent to upward current field lines which are closed by the downward current.

[3] Ionospheric electrons at the base of a downward current flux tube are accelerated out into the magnetosphere as a highly collimated electron beam. This results in some depletion of the ionospheric plasma, but no visible aurora. The details of electron acceleration are still an area of active research. Some spacecraft observations show excellent coincidence of electron beam energy with electric potential (found from integrating \mathbf{E} along the spacecraft trajectory). This suggests a quasi-steady acceleration mechanism with U-shaped potential contours [Carlson *et al.*, 1998b], with much of the acceleration occurring below the B/n peak (\mathbf{B} and n being the magnetic field and electron number density, respectively),

e.g., *Temerin and Carlson* [1998] and *Cran-McGreehin and Wright* [2005a, 2005b]. However, other events seem to be associated with upward moving double layers, suggesting a time-dependent process [Andersson *et al.*, 2002; Andersson and Ergun, 2006; Ergun *et al.*, 2003].

[4] Recent work by *Hwang et al.* [2006a, 2006b] suggests that the majority of downward current channels are curved, rather than straight (i.e., they are not translationally invariant in the East-West direction). There is considerable variation, but there is a bias for strong \mathbf{E}_\perp structures to be straight, and the wider (in latitude, >300 km) current channels to be curved. The latter appear to be consistent with U-shaped potential contours, while the narrower (<150 km) structures have some contours extending down to the E-region. (The widths quoted here were measured at FAST altitudes of between 2500 km and 4100 km.)

[5] The upward and downward currents are connected through Pedersen and Hall currents that flow in the ionosphere. Note that in quasi-steady situations where the electric field may be represented in terms of a scalar potential, the Hall current does not contribute to the global current closure as the Hall current is itself divergence-free. The ionosphere (roughly the region below the B/n peak) is an important component in the global circuit and can lead to the trapping of unstable Alfvén waves in the Ionospheric Alfvén Resonator [Lysak and Song, 2002] which may lead to the development of small scale structures [Streltsov and Lotko, 2004, 2005].

[6] The removal of ionospheric electrons to feed the downward current leg can cause significant modification to the ionosphere. *Aikio et al.* [2002, 2004] observed substantial reduction in E-region electron number density, while the energy of the upgoing electron beam increased

¹Mathematical Institute, University of St. Andrews, St. Andrews, Fife, Scotland.

²University College London, Mullard Space Science Laboratory, Holmbury St. Mary, Dorking, Surrey, UK.

³Space Sciences Laboratory, University of California, Berkeley, California, USA.

⁴CCLRC Rutherford Appleton Laboratory, Chilton, Didcot, Oxfordshire, UK.

from 200 to 1000 eV over 70 s as the current became established. *Marklund et al.* [2001] observed longer time evolution of a downward current channel (~ 300 s) with the Cluster mission. They saw how the current sheet needed to broaden in latitude to have access to more electrons as the ionospheric electrons became depleted. Moreover, the total current seemed to remain constant throughout the event, but the current density and electron beam energy dropped toward the end of the observations, consistent with the current channel broadening and modeled current-voltage relations [*Temerin and Carlson*, 1998; *Cran-McGreehin and Wright*, 2005a, 2005b].

[7] Quasi-neutral current continuity will allow the local electron and ion number densities to change while maintaining a vanishing total charge density. Hence the number of electrons in the ionosphere will be reduced on field lines carrying a downward current at altitudes where the Pedersen current flows (mainly the E and lower F regions). The electrons move along the magnetic field line and carry the field-aligned current, while the ions move horizontally and carry the Pedersen current. The combined current is divergence-free and allows the plasma to stay quasi-neutral. This feature has been demonstrated in detailed modeling of the ionosphere in which the magnetosphere is represented as a prescribed current at the upper boundary of the ionosphere. Estimates of the evacuation time range from a few seconds for strong currents ($10 \mu\text{Am}^{-2}$) [*Karlsson and Marklund*, 1998] to 30 s for weaker currents ($0.02 \mu\text{Am}^{-2}$) [*Doe et al.*, 1995]. More recently the magnetosphere has been included self-consistently in numerical [*Streltsov and Marklund*, 2006] and analytical [*Cran-McGreehin et al.*, 2007] models which exhibit latitudinal broadening of the downward current layer consistent with that reported by *Marklund et al.* [2001].

[8] The structure of the downward current region in latitude and longitude is not easy to investigate as the signature in this region has yet to be verified. Upgoing electron beams have a latitudinal scale of several tens of km (when mapped to the ionosphere), and are likely to be as extended in longitude as visible auroral arcs are, particularly since the downward current region may on occasion be sandwiched between two visible extended arcs [*Aikio et al.*, 2004].

[9] For downward currents, it is not clear how two-dimensional cross-sectional structure (perpendicular to \mathbf{B}) maps from the ionosphere to the magnetosphere. FAST-SuperDARN conjunctions have shown how large latitudinal scales in the ionosphere (several 100s km) contain fragmented structures of ~ 50 km at 4000 km altitude [*Scofield et al.*, 2005, 2007]. Whether these fragmented structures are translationally invariant in longitude, or isolated flux tubes, is not clear.

[10] In this paper we present data from a conjunction of FAST and Cluster which address how upgoing ionospheric electron beams map over the altitude range from 3000 km to $4 R_E$. Section 2 presents the satellite data for the conjunction showing that most of the electron acceleration has occurred below FAST, and suggesting that j/B is conserved along field lines. Section 3 models the expected signature at Cluster for isolated flux tubes of circular cross-section carrying the current (i.e., current filaments), and shows

good agreement with the Cluster observations. Section 4 discusses the results and concludes the paper.

2. Satellite Data

2.1. Cluster Data

[11] At around 12 UT on 7 January 2003, the 4 Cluster spacecraft were passing through perigee ($\sim 4.5 R_E$), at ~ 4 MLT. At this time the spacecraft were separated along the orbit, in a “string-of-pearls” configuration, in which spacecraft 1 (hereafter C1) was furthest along the orbital track, followed by C2, C4 and finally C3. At this time, the along-orbit separations were of the order of $2.66 R_E$ (C1–C3), $2.11 R_E$ (C2–C3) and $1.36 R_E$ (C4–C3). Following perigee in the dawn side inner magnetosphere, the spacecraft moved northward and duskward over the next few hours.

[12] The PEACE instruments on each of the Cluster spacecraft are designed to measure the 3-D fluxes of electrons in the energy range 0.6 eV to 26 keV [e.g., *Johnstone et al.*, 1997]. The instruments are turned off during the perigee pass due to the susceptibility of the sensors to penetration and damage by MeV electrons from the radiation belts, and are turned on once the individual spacecraft pass a limiting altitude. Figure 1 shows data recorded by the PEACE instruments on each of the 4 spacecraft during the period 1200–1400 UT, as they each emerge from perigee. Each of the first 4 panels of this figure shows an energy–time spectrogram covering the range from 10 eV to 30 keV during this period, with the differential energy flux of electrons with a pitch angle of 180° in this energy range indicated by the color bar. Although the instruments on the leading spacecraft (C1, top panel) are turned on before the start of the period shown, those on the trailing spacecraft are not turned on until ~ 1215 (C2, second panel), 1235 (C4, 4th panel) and 1307 UT (C3, 3rd panel), resulting in the data gaps before those times in the respective plots. Note that the ephemeris data at the bottom of the figure refer to the position of C3, which is generally used as the reference spacecraft by the Cluster community. Note also that the solid trace which is apparent in the top 2 panels represents the value of the spacecraft potential, which is seen to reach values >10 V during the period shown. The operation of the ASPOC potential control device [*Torkar et al.*, 2005] on Cluster 3 and 4 holds the spacecraft potential below the levels shown in these panels. Note that the high fluxes of electrons that are recorded near or below this spacecraft potential level are photoelectrons emitted by the spacecraft, and are not representative of the ambient plasma populations. They are ignored in all subsequent analyses and discussions in this paper.

[13] Note that in the periods immediately following the start of data acquisition on each spacecraft, when each spacecraft is located at relatively low-latitude, the PEACE instruments detect a population of electrons of relatively high energy (~ 10 keV), which indicate that the spacecraft are sampling the trapped electron populations of plasma sheet origins on closed field lines in the inner magnetosphere. By the end of the interval shown, this population has completely disappeared at each of the 4 spacecraft, indicating that they have each moved onto open lobe field lines above the polar cap. The crossing of the open-closed field line boundary (OCB) occurs around 1248 UT for C1,

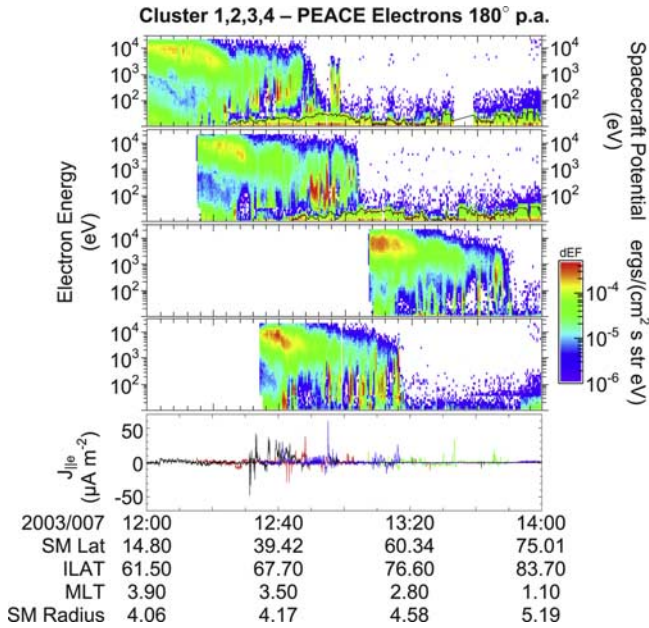


Figure 1. Cluster PEACE data for the period 12–14 UT on 7 January 2003. The first 4 panels show energy-time spectrograms for the differential energy flux of 180° pitch angle electrons detected at each of the 4 Cluster spacecraft (C1 to C4, top to bottom respectively). The energy range covered is 10 eV to 30 keV, with the differential energy flux indicated by the color bars to the right of the figure. Solid traces in the top 2 panels indicate the spacecraft potential, which is >10 V on C1 and C2 at this time. The bottom panel indicates the net parallel current detected at each spacecraft determined from the electron flux (C1, black; C2, red; C3, green; and C4, blue), while the ephemeris data below the figure are for C3, the reference spacecraft. Note the sporadic observation of electrons with energies up to ~ 1 keV around the time of the OCB crossing by each spacecraft, and their association with enhanced field aligned currents of a few 100 nAm^{-2} .

1304 UT for C2, 1316 UT for C4, and finally at 1348 UT for C3. For each of these cases, the spacecraft were located within the ILAT range 74° – 76° and within the range 2.9–3.2 MLT.

[14] Note also that as each spacecraft approaches the OCB, they begin to detect more structured field-aligned electron populations of lower energy (up to 1 keV) but somewhat higher differential energy flux. Note that these populations provide a highly structured electron current region, as indicated in the bottom panel of Figure 1, which shows the net parallel current carried by the electrons in the PEACE energy range during these crossings of the OCB. (It is not possible to compare this current with one derived from the magnetic field gradients between the four spacecraft because of their linear alignment.) In this panel, the traces from each spacecraft are color coded, with data from C1 in black, C2 in red, C3 in green and C4 in blue. From this panel it is evident that the <1 keV electron populations often carry significant, but sporadic current, reaching several 100 nAm^{-2} .

[15] Figure 2 shows a more detailed look at the data recorded by the PEACE instrument on C4. This figure

covers the period 1235–1320 UT on 7th January 2003, and thus focuses in on the interval just prior to the C4 crossing of the OCB. The three panels in this figure represent spectrograms showing the differential energy flux of particles with pitch angles of 0° , 90° and 180° , from top to bottom respectively. This figure illustrates that much of the structure in the 30 eV–1 keV electron populations between 1253 and 1317 UT is confined to the 180° pitch angle particles, i.e., the upgoing electrons moving anti-parallel to the field. Note particularly that a clear beam of upward moving electrons was detected on C4 at ~ 1305 UT. This is of particular interest here, since, as we discuss in the next section, C4 was in very close magnetic conjunction with the FAST satellite, located at lower altitudes. At this time the ratio of the integrated electron flux at C4 to the observed magnetic field strength is $\sim 0.1 \text{ Am}^{-2} T^{-1}$. This quantity is conserved along a field line carrying a steady field-aligned current, and so can be directly compared with measurements recorded by FAST at the time of conjunction.

2.2. Fast Data

[16] On 7 January 2003 between 13:00 and 13:10 FAST was traveling northward from 63° to 81° invariant latitude at ~ 3.2 h MLT and an altitude around 3200 km. The hot (up to 10 keV) isotopic electrons of the plasma sheet are clearly visible between 13:01 and 13:06:30 UT in panels 1, 2, 3 and 4 of Figure 3. The transition from plasma sheet to lobe is accompanied by some interesting structure in the electron distributions. At 13:04 UT panels 1–4 show an enhancement of downgoing electrons at an energy of $\sim \text{keV}$ probably associated with an inverted-V structure.

[17] Between 13:05 and 13:07 UT there are enhanced field-aligned electron fluxes with energies of around 100 eV. Panel 4 shows these to be highly collimated. The feature we shall focus on is the upward electron beam at 13:05:40 UT indicated by the red spot in panel 4 at 180° pitch angle. This is of particular interest because at this time Cluster 4 had a magnetic conjunction with FAST and also observed an upward electron beam. The latitudinal extent of the upgoing electron beam is roughly 30–40 km at an altitude of about 3200 km.

[18] Given that the traveltime of 100 eV electrons between FAST and Cluster is a few seconds, we would expect the total upward electron flux on a magnetic flux tube connecting the spacecraft to be similar. In terms of the current carried by these electrons, we expect j/B to be conserved. The magnetic field strength measured by the flux-gate magnetometer (not shown) was 17×10^3 nT, and during the upward electron beam encounter at 13:05:40 UT j varies from 0 to $5 \mu\text{Am}^{-2}$, meaning j/B increases from 0 to a maximum of $0.3 \text{ Am}^{-2} T^{-1}$. At the same time, the value of j/B at Cluster 4 is $0.1 \text{ Am}^{-2} T^{-1}$ ($j \approx 0.05 \mu\text{Am}^{-2}$ and $B \approx 550$ nT), and so lends support to the interpretation that Cluster and FAST are in a magnetic conjunction.

2.3. Scales in the Ionosphere

[19] The field aligned electron burst seen by Cluster and FAST have structure on a range of scales. To provide a ready comparison between the two data sets, we map the latitudinal extent of the beams to the ionosphere (100 km altitude) along magnetic field lines. For Cluster this trans-

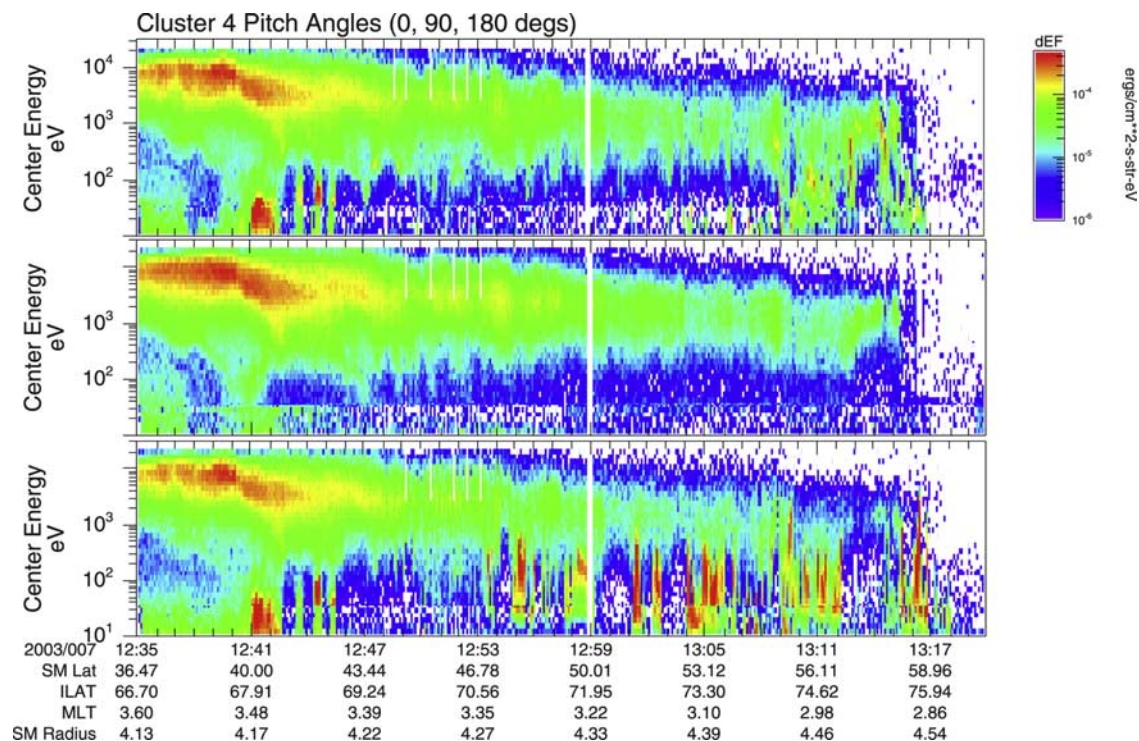


Figure 2. PEACE data from C4 for the period 1235–1320 UT on 7 January 2003. The 3 panels show energy-time spectrograms for the differential energy flux of 0° , 90° and 180° pitch angle electrons, from top to bottom, respectively. Note that structured upward electron beams (180° pitch angle) are prevalent from ~ 1253 – 1317 UT. Note particularly that upward moving electrons are seen at ~ 1305 UT, when C4 is in close magnetic conjunction with the FAST spacecraft.

lates to 1 s of observing time being equivalent to 0.42 km in the ionosphere. For FAST the mapping is $1 \text{ s} \equiv 3.4 \text{ km}$.

[20] Both Cluster and FAST see the finest structure at the resolution of data collection. For FAST (80 ms) and Cluster (4 s) these correspond to latitudinal scales in the ionosphere of 300 m and 1.5 km, respectively. However, it is also evident from the data that the electron beams are organized into bundles of current filaments. For Cluster, an isolated bundle lasts for ~ 40 s, and contains filaments lasting ~ 20 s (18 km and 9 km, respectively, in the ionosphere). For FAST the downward current beam at conjunction lasts 6.6 s and contains filaments lasting 0.6–1.7 s. The corresponding scales in the ionosphere are 21 km and 1.8–6 km, respectively. For both spacecraft it appears that the isolated bundles have similar scales in the ionosphere of ~ 20 km.

3. Interpretation and Modeling

[21] Two extreme scenarios exist that may explain the bursts of field-aligned electrons seen by Cluster. In the first, Temporal Structuring, we attribute the bursts of electrons seen by Cluster as a switching on and off of the beam at the lower altitude source. In this case the width of the current carrying flux tube could cover the entire invariant latitude range over which the beams are seen, but be modulated in time. The second scenario, Spatial Structuring, regards the beams as being independent of time, but fragmenting into current filaments as they extend away from the Earth. Even if these beams do not change in time, the motion of Cluster through these filaments will give rise to a switching on and

off of the observed electron flux as the spacecraft enters and exits a filament.

[22] In nature both temporal and spatial variations will occur, but we shall see one is dominant for the data here. In the case of Temporal Structuring (switching the beam source on and off), it is likely that the higher energy electrons will arrive first and the lower energies later, suggesting a velocity dispersion signature may be evident. The traveltime of ~ 100 eV electrons from FAST to Cluster is a matter of seconds. Given that the sampling rate at Cluster is 4 s, it is not possible to be confident about identifying the presence or absence of velocity dispersion.

[23] Another feature that may help decide between Temporal Structuring and Spatial Structuring is the correlation of the magnetic field fluctuation with electron flux. Since the electron beam carries a current, there will be a magnetic field ($\nabla \times \mathbf{b} = \mu_0 \mathbf{j}$) associated with it. If the source is switched on and off, the magnetic field should also switch on and off with the observed electron flux. However, if the beams are spatially structured and steady in time we would expect to see the magnetic field signature existing outside of the beam filament: Each filament would be surrounded by a magnetic field like that around a current-carrying wire.

3.1. Modeling

[24] Figure 4a shows an array of 6 current filaments, with x and y representing local coordinates perpendicular to the background magnetic field. An individual filament carries a uniform current density and is normalized to have a corresponding magnetic field amplitude of unity on the

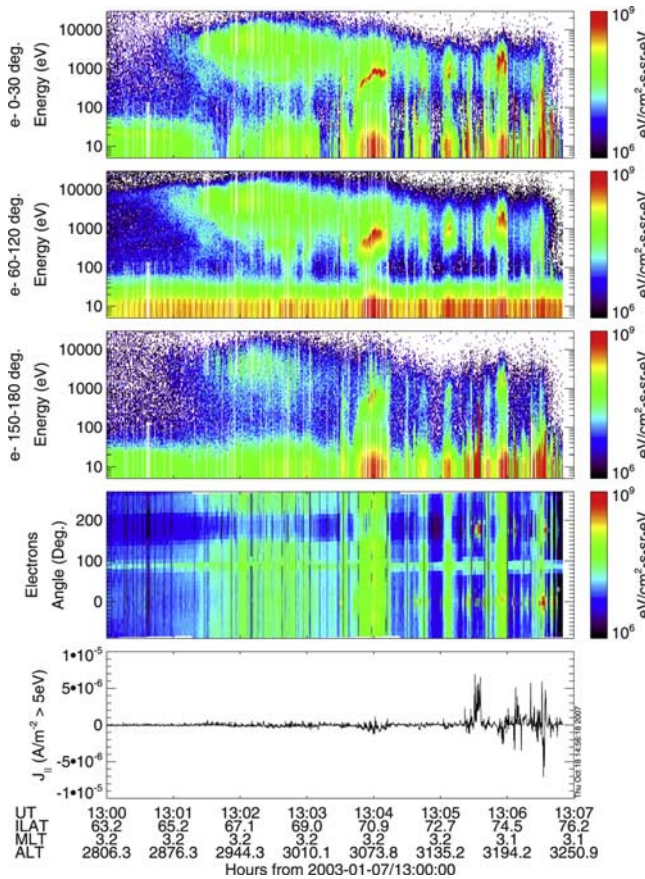


Figure 3. Electron data recorded by FAST on 7 January 2003. The top three panels show electron energy spectra for downgoing, $\sim 90^\circ$ degree pitch angle, and upgoing electrons, respectively. The fourth panel shows the pitch angle distribution. Note the enhancement at 13:05:40 UT which corresponds to upgoing electrons carrying a strong field aligned downward current (bottom panel).

surface of the filament. Note that the magnetic field associated with current filaments is perpendicular to the background magnetic field (i.e., $b_z = 0$).

[25] The straight line in the figure represents the transit of a Cluster spacecraft through the array of filaments, of which it intersects three. Figure 4b shows the field observed by the spacecraft during its transit. The bottom panel is the normalized electron flux which increases from a small background value when the spacecraft is inside a filament. Note how the magnetic field perturbation is present even when the spacecraft is not inside a filament.

[26] Figure 4c shows the (b_x, b_y) hodogram for the satellite transit. The entry and exit of the first tube are labeled *A* and *B*, while those for the second and third tube are *C*, *D* and *E*, *F*, respectively. The magnetic signatures show many features that are qualitatively similar to Cluster field observations. However, it is difficult to get an exact correspondence because there may be filaments nearby that the spacecraft does not intersect but for which it does see a magnetic signature. For this reason the unambiguous interpretation of the data is not possible.

[27] To minimize the complications introduced by nearby filaments we shall model the signature of a solitary current

filament encounter, and compare with Cluster data for a relatively isolated beam transit. Figure 5a shows the hodogram for such a filament crossing. At large distances from the tube $(b_x, b_y) \rightarrow 0$, and these fields grow as the tube is approached. Interestingly, the hodogram is a circle if the spacecraft trajectory does not intersect the filament. If the tube radius is a_0 , and the magnetic field amplitude b_0 at the tube surface, then the radius of the circle is $(a_0 b_0 / 2a)$, where a is the closest approach distance to the tube axis. The long-dashed line has a closest approach of $3.0a_0$, while the short-dashed line approaches closer to $1.2a_0$ and sees correspondingly larger magnetic fields.

[28] The solid line in 5a is the hodogram for a trajectory that intersects the current filament. While the spacecraft is outside the beam we see the usual circular character in the hodogram. However, at *A* the spacecraft enters the tube and remains inside it until *B*. The fact that the straight line connecting *A* and *B* is at constant b_x means the spacecraft is traveling in the x direction. If this orientation were changed, the hodogram would simply be rotated about the origin.

[29] That the line joining *A* and *B* in Figure 5a is a straight line is a result of our choice of uniform current density inside the tube. Figure 5b reproduces this trace for a closest approach of 0.5, but also others where the current density is a function of distance (r) from the tube axis. The short-dashed line ($j \propto 1 - (r/a_0)^2$) has the current density fall to zero at the tube surface, whereas the long-dashed line ($j \propto (r/a)^2$) has it increase from zero at the tube axis. Outside of the tube the hodograms all coincide, but the details inside the tube differ.

3.2. Cluster 3 Data

[30] The FAST/Cluster-4 conjunction discussed earlier give a somewhat complicated magnetic signature in the

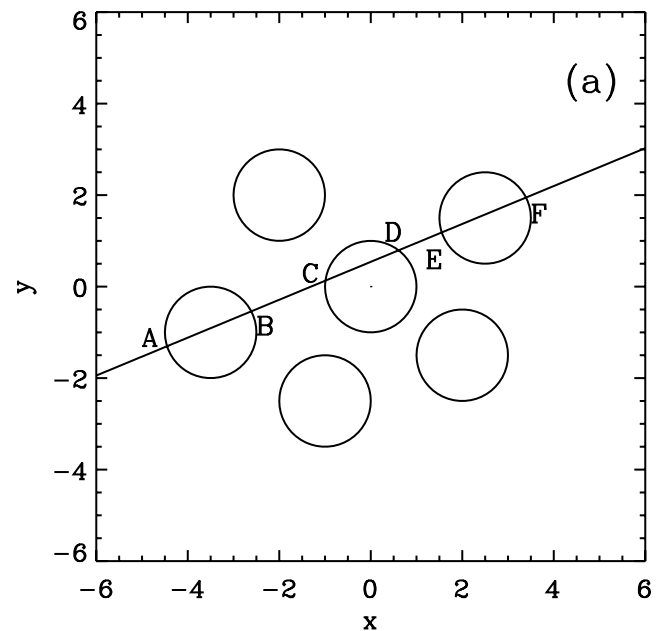


Figure 4a. Modeled signature of a Cluster spacecraft flying through an array of current filaments. The trajectory of the spacecraft (solid line) intersects three current-carrying flux tubes.

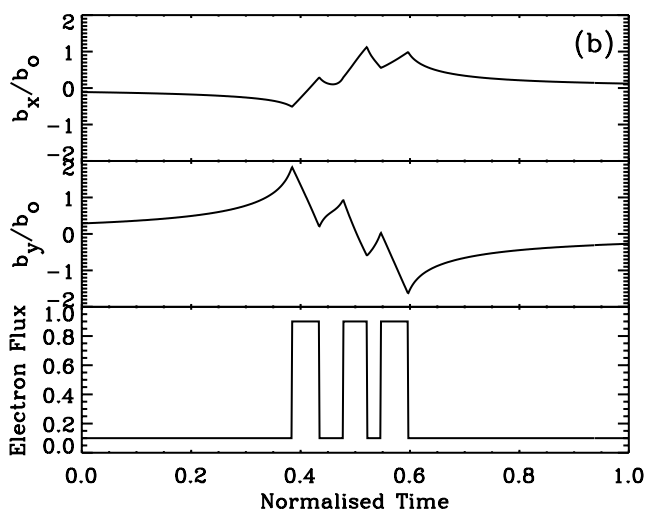


Figure 4b. The time history of the two magnetic field components (b_x , b_y) perpendicular to the flux tube, and the normalized beam electron flux.

Cluster-4 magnetometer data, that while qualitatively similar to Figure 4b, does not permit a rigorous comparison with our modeling. This is probably due to the presence of neighboring filaments that are not intersected, and individual filaments not having circular cross-sections, etc. To minimize these problems we seek an encounter of one of the Cluster spacecraft with a relatively isolated electron beam, and then compare the hodogram with the modeled one shown in Figure 5.

[31] In Figure 6 we consider the magnetic variations that are associated with the electron structure observed by the PEACE instruments on spacecraft C3, covering the period 1300–1400 UT on 7 January 2003. The top 4 panels of this figure show the 3 components and the magnetic field strength measured by the FGM instrument of C3 (black trace) together with the variation in these parameters expected on the basis of evaluating the Tsyganenko magnetic field model T96 [Tsyganenko, 1995] at the C3 position for the prevailing solar wind and magnetospheric conditions. Note that the scale used in the fourth panel, showing $|\mathbf{B}|$, has a much smaller range (60 nT) on the vertical axis compared to the components in the first 3 panels, which each cover a range of 500 nT. Hence it can be seen that although the individual components vary by up to several 100 nT in the interval shown, the variation in field strength is only ~ 50 nT. Moreover, it can be readily seen that the measured $|\mathbf{B}|$ does not show significant higher frequency fluctuations above that of the global trend indicated by the T96 model. Such fluctuations are clearly limited to ~ 1 nT or less.

[32] Panel (e) of Figure 6 shows the difference between the measured field vector and the T96 model, with the 3 components dB_x , dB_y , and dB_z represented by the black, red and green traces respectively. These data indicate that significant fluctuations, in the amplitude range 5–10 nT, occur in these components between ~ 1315 UT and 1350 UT. Since these fluctuations do not occur in concert with $|\mathbf{B}|$ fluctuations, they clearly must occur in the direction perpendicular to the main field ($|\mathbf{B}| \sim 580$ nT). The bottom panel of this figure shows the spectrogram of the differential

energy flux of electrons with pitch angles of 180° , i.e., the upgoing electrons moving anti-parallel to the field recorded by the PEACE instrument on C3 during this period. This panel shows a clear association between the magnetic fluctuations and the appearance of the upgoing electrons just prior to this spacecraft crossing the OCB. Note particularly the isolated beam appearing just after 1341 UT which is associated with an inflection in all 3 components of $d\mathbf{B}$.

[33] This is further illustrated in Figure 7, which shows the results of performing a minimum variance analysis (MVA) on the $d\mathbf{B}$ fluctuation cycle which occurred between 1338 UT and 1342 UT. This analysis returns a minimum variance coordinate system in which the minimum, intermediate and maximum variance directions are $\mathbf{n}_3 = (-0.658, -0.67, 0.344)$, $\mathbf{n}_2 = (-0.334, 0.669, 0.664)$ and $\mathbf{n}_1 = (-0.675, 0.322, -0.644)$ respectively, with well separated eigenvalues ($\lambda_2/\lambda_3 = 63$; $\lambda_1/\lambda_2 = 21$). Note that $\mathbf{n}_3 \cdot \mathbf{B}/B = 0.998 \approx 1$, confirming that the direction of minimum variance is indeed along the main magnetic field direction. The top-left, top-right and bottom-left panels of Figure 7 show the hodograms tracing the ‘movement’ of the $d\mathbf{B}$ vector in the derived MVA coordinate system, showing the projection in the maximum-intermediate, maximum-minimum, and minimum-intermediate planes respectively. The 3 panels in the bottom-right of the figure show the variation of $d\mathbf{B}$ in the maximum, intermediate and minimum variance directions respectively. These panels show that the magnetic variations are confined to the intermediate and maximum directions (and thus perpendicular to the main field), with a bipolar signature occurring in the maximum variance direction and a small peak in the intermediate direction. In the derived frame there is no residual field in the minimum variance direction. Note that, as evident in the bottom panel on Figure 6, there are several variance cycles in $d\mathbf{B}$ in the period of interest. Although not shown here, similar MVA analyses on other cycles returns essentially the

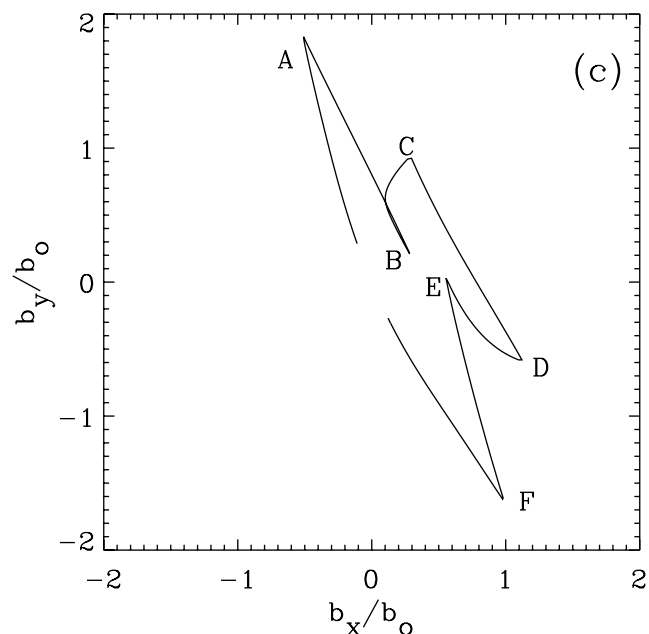


Figure 4c. Hodogram of ($b_x(t)$, $b_y(t)$) for the transit.

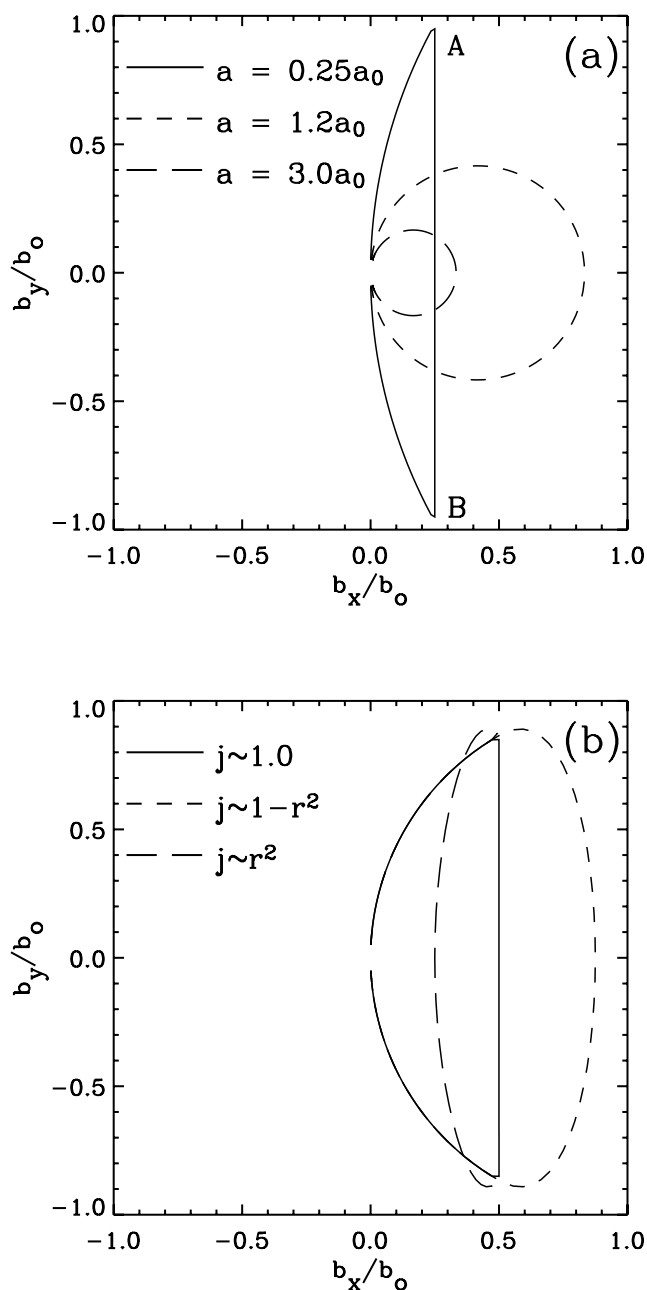


Figure 5. Hodogram of $(b_x(t), b_y(t))$ for a transit of a single current filament. The filament has a radius a_0 and surface perturbation magnetic field b_0 . In (a) the solid line corresponds to a trajectory that enters (A) and exits (B) the electron beam and has a closest approach to the tube axis of $0.25a_0$. The filament is assumed to carry a spatially uniform current density. The dashed lines correspond to paths remaining outside the filament. (b) The spacecraft trajectory approaches to $0.5a_0$ of the tube axis. Hodograms for three different current profiles are plotted.

same results as that obtained for the sub-period discussed here.

3.3. Cluster 3 Interpretation

[34] Figure 6 (panel e) shows that the fluctuations of magnetic field have an amplitude of 5–10 nT. The rapid

excursions in these fluctuations at 13:32–13:33, 13:35–13:36, 13:39–13:41, 13:43–13:43:30, 13:45–13:46, 13:47–13:47:30 and 13:49–13:50 correspond exactly with the electron enhancements seen by Cluster 3 in panel *F* (reproduced from the 3rd panel of Figure 1) and are qualitatively similar to the modeled b_x and b_y signatures in Figure 4b. We also see that $|\mathbf{B}|$ (shown in the fourth panel of Figure 6) shows fluctuations of less than 1 nT, and this is

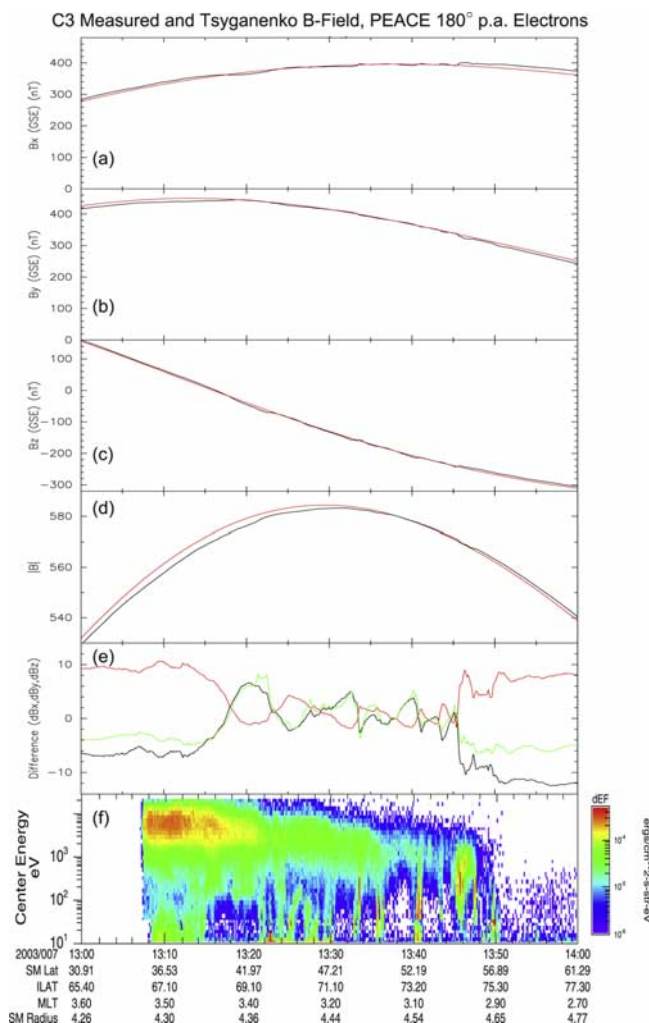


Figure 6. Panels (a)–(d) Magnetic field measurements by C3 (black traces) for the period 1300–1400 UT on 7 January 2003, together with the magnetic field derived from an application of the Tsyganenko T96 model to the C3 location and prevailing solar wind and magnetospheric conditions (red trace). Note the range of the vertical axis in panel (d) is rather narrower than for the components B_x , B_y , and B_z shown in the upper 3 panels respectively. Panel (e) The difference vector between the measured and T96-derived magnetic field, showing dB_x (black trace), dB_y (red trace) and dB_z (green trace). Note the occurrence of magnetic fluctuations of amplitude 5–10 nT in all 3 components of this difference vector during the period ~ 1315 – 1350 UT. These far exceed fluctuations in $|\mathbf{B}|$ (~ 1 nT, panel (d)), and thus can be attributed to magnetic disturbances in the direction perpendicular to the main field.

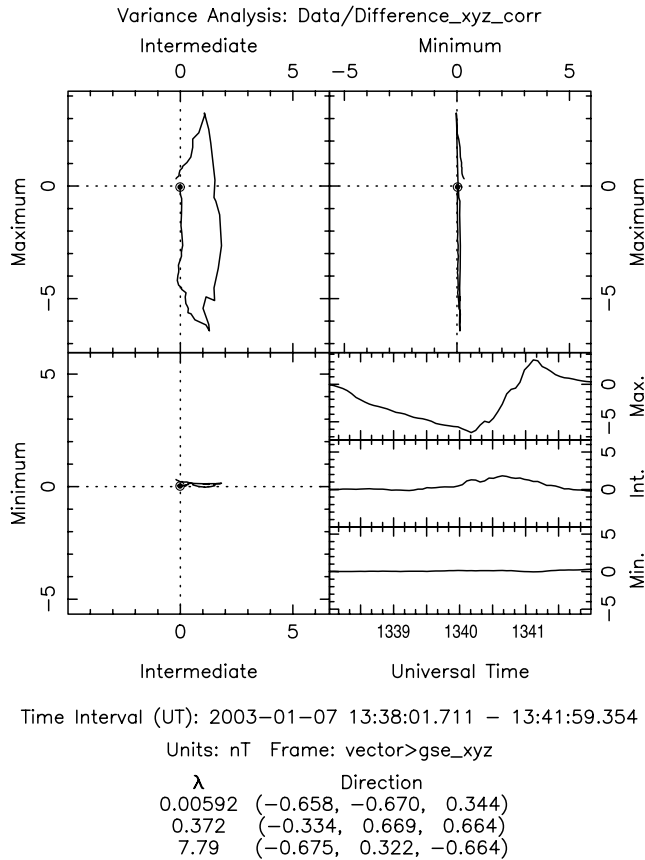


Figure 7. Panels (a)–(c) Hodograms of the variation of the difference vector δB for the period 1338–1342 UT when transformed into a minimum variance coordinate system. The MVA coordinate system is well defined and is as indicated at the bottom of the figure, with the minimum variance direction very closely aligned with the main field direction. Panels (d)–(f) show the difference vector variations in the maximum, intermediate and minimum variance directions respectively.

in accord with our expectations that the 5–10 nT fluctuations should be perpendicular to the background field.

[35] The electron beam seen by Cluster 3 at 13:40–13:41 UT (Figure 6, panel f) is relatively isolated, and the hodogram (shown in Figure 7) taken over 13:38–13:42 UT shows entry and exit signatures in the intermediate and maximum (similar to b_x and b_y) field components as expected from the modeling. The time history of the maximum component is crucial as it shows unambiguously that the magnetic field disturbance is present before ($t < 13:40$) and after ($t > 13:41$) the beam encounter (13:40–13:41), during which time the field trace changes sign as seen in the model results. (See, e.g., the b_y signature in Figure 4b.) This indicates that the current carrying electron beam is present even when the spacecraft is not embedded in a filament.

[36] From this we conclude that the electron beam is quasi-steady on the transit time of a Cluster spacecraft, suggesting that the observed periodic enhancements in electron flux are due to spatial structuring rather than a time-dependent beam source. It is interesting that the

upward electron beam encountered by FAST is probably just one of the beams traversed by Cluster.

[37] For a hodogram with the orientation in Figure 5a we can use the values of the magnetic field at entry and exit to estimate the normalized closest approach to the tube axis (a/a_0) from

$$\frac{a}{a_0} = \frac{|b_x/b_y|}{\sqrt{1 + b_x^2/b_y^2}} \quad (1)$$

From Figure 7 the magnetic field ratio $|b_x/b_y|$ at entry and exit is roughly 0.2 and 0.33, suggesting the closest approach (a/a_0) was between 0.2 and 0.3. Of course, real current filaments will not be exactly circular, and there may be field contributions from neighboring filaments meaning the entry and exit estimates are not identical. Nevertheless, both estimates indicate that Cluster 3 penetrated deep inside the electron beam.

4. Discussion and Summary

[38] The perpendicular scale of a current filament may be estimated simply from Cluster’s speed perpendicular to B ($\sim 2.5 \text{ km s}^{-1}$) and the duration of the beam (30 s – 1 min), suggesting a scale of 70–150 km. Thus the radius of a filament is $a_0 = 35\text{--}75 \text{ km}$, from which it is possible to calculate the magnetic field perturbation amplitude (b_0) given the current density in the filament. The latter is typically $0.05 \mu\text{A m}^{-2}$ at Cluster (based upon electron flux measurements), and implies $b_0 = \mu_0 j a_0 \approx 5 \text{ nT}$, in agreement with the field perturbations seen in Figures 6 and 7.

[39] If a circular current tube of perpendicular extent, say, 100 km, is mapped from Cluster ($B = 550 \text{ nT}$) to FAST ($B = 17 \times 10^3 \text{ nT}$) the corresponding size is 18 km, which is similar to the upward electron beam scale seen by FAST. The current filaments at Cluster are often grouped in bundles that take up to a few minutes to transit, suggesting a width of $\sim 500 \text{ km}$. The entire time interval over which the beams occur is about 30 min, and corresponds to a width of $\sim 1R_E$ at Cluster.

[40] The picture that emerges is of current mapping from the ionosphere as discrete filaments, as the electrons carrying the current trace out magnetic field lines. On the timescale for Cluster to transverse a filament (30 s–1 min) the current appears to be steady. However, observations by *Marklund et al.* [2001] indicate that upward electron beams may have a lifetime of about 4 min, determined by the ability of the ionosphere to supply the required electrons [*Streltsov and Marklund, 2006; Cran-McGreehin et al., 2007*]. It is certainly the case that for the hour duration over which the Cluster spacecraft observed upgoing electron beams, the details of beam location and current strength would change considerably. It is likely that some filaments would fade away, while new ones would emerge.

[41] The above scenario is also consistent with the fact that the four Cluster spacecraft data in Figure 1 are not a simple replication of one another with a shift in time. Indeed, we could find no correlation in the detailed features of the beams between spacecraft. The interval between beams is generally greater than duration of a beam, and this suggests that space is filled by well separated current

tubes. Hence different spacecraft will generally encounter different filaments. Moreover, allowing for the fact that individual filaments may only have a lifetime of a few minutes, we expect the correlations between different spacecraft to be reduced even further. We also note that the lack of correlation argues against the possibility of the switching on and off in time of a broad layer (1000 km in the ionosphere) of downward current that engulfs all the Cluster spacecraft.

[42] It is interesting to note that the perpendicular scale of the beam seen by FAST and that at Cluster (when mapped to FAST altitudes) are both several 10s of km. (When mapped to the ionosphere, the size is 10–20 km.). We do not have an explanation for this scale, but note it is the same as that reported by Scofield *et al.* [2005, 2007], in their studies of conjunctions between SuperDARN and FAST. The large-scale latitudinal structure of the currents (based upon SuperDARN) were between 150 and 1300 km. However, the currents seen by FAST had fine structure on a scale of 50 km (corresponding to about 30 km in the ionosphere). Scofield *et al.* suggested the structure was due to electron inertial effects, and this could also be important in gaining an understanding of the origin of current filament size we report here. Recent modeling by Streltsov [2007] shows how the Ionospheric Alfvén Resonator can naturally develop fine structure in the field aligned current of 10–20 km in the ionosphere in the downward current channel. The extension of these features out into the magnetosphere is favored when the Alfvén and Pedersen conductances are similar. This condition is also favorable for the growth of Ionospheric Alfvén Resonator instability that produces the fine structure, and could lead to similar signatures in satellite data to those we report.

[43] **Acknowledgments.** Cluster data analysis was done with the QSAS science analysis system provided by the United Kingdom Cluster Science Centre (Imperial College London and Queen Mary, University of London) supported by The Particle Physics and Astronomy Research Council (PPARC). FAST data analysis was funded by NASA grant NAG5–3596, and CCC supported through NASA grant NNG06GG63G. ANW is grateful to Bob Lysak and Anatoly Streltsov for helpful discussions.

[44] Amitava Bhattacharjee thanks Kyoung-Joo Hwang and Kristina Lynch for their assistance in evaluating this paper.

References

- Aikio, A. T., T. Lakkala, A. Kozlovsky, and P. J. S. Williams (2002), Electric fields and currents of stable drifting auroral arcs in the evening sector, *J. Geophys. Res.*, *107*(A12), 1424, doi:10.1029/2001JA009172.
- Aikio, A. T., K. Mursula, S. Buchert, F. Forme, O. Amm, G. Marklund, M. Dunlop, D. Fontaine, A. Vaivads, and A. Fazakerley (2004), Temporal evolution of two auroral arcs as measured by the Cluster satellite and coordinated ground-based instruments, *Ann. Geophys.*, *22*, 4089.
- Andersson, L., and R. E. Ergun (2006), Acceleration of antiearthward electron fluxes in the auroral region, *J. Geophys. Res.*, *111*, A07203, doi:10.1029/2005JA011261.
- Andersson, L., R. E. Ergun, D. L. Newman, J. P. McFadden, C. W. Carlson, and Y.-J. Su (2002), Characteristics of parallel electric fields in the downward current region of the aurora, *Phys. Plasmas*, *9*(8), 3600, doi:10.1063/1.1490134, 2002.
- Carlson, C. W., et al. (1998a), FAST observations in the downward auroral current region: Energetic upgoing electron beams, parallel potential drops, and ion heating, *Geophys. Res. Lett.*, *25*, 2017.
- Carlson, C. W., R. F. Pfaff, and J. G. Watzin (1998b), The Fast Auroral SnapshoT (FAST) mission, *Geophys. Res. Lett.*, *25*, 2013.
- Cran-McGreehin, A. P., and A. N. Wright (2005a), Electron acceleration in downward auroral field-aligned currents, *J. Geophys. Res.*, *110*, A10S15, doi:10.1029/2004JA010898.
- Cran-McGreehin, A. P., and A. N. Wright (2005b), Current-voltage relationship in downward field-aligned current region, *J. Geophys. Res.*, *110*, A10S10, doi:10.1029/2004JA010870.
- Cran-McGreehin, A. P., A. N. Wright, and A. W. Hood (2007), Ionospheric depletion in auroral downward currents, *J. Geophys. Res.*, *112*, A10309, doi:10.1029/2007JA012350.
- Doe, R. A., J. F. Vickrey, and M. Mendillo (1995), Electrodynamic model for the formation of auroral ionospheric cavities, *J. Geophys. Res.*, *100*(A6), 9683.
- Ergun, R. E., L. Andersson, C. W. Carlson, D. L. Newman, and M. V. Goldman (2003), Double layers in the downward current region of the aurora, *Nonlinear Proc. Geophys.*, *10*, 45.
- Hwang, K.-J., K. A. Lynch, C. W. Carlson, J. W. Bonnell, and W. J. Peria (2006a), Fast auroral snapshot observations of perpendicular DC electric field structures in downward auroral current regions: Morphology, *J. Geophys. Res.*, *111*, A09205, doi:10.1029/2005JA011471.
- Hwang, K.-J., K. A. Lynch, C. W. Carlson, J. W. Bonnell, and W. J. Peria (2006b), Fast auroral snapshot observations of perpendicular DC electric field structures in downward current regions: Implications, *J. Geophys. Res.*, *111*, A09206, doi:10.1029/2005JA011472.
- Johnstone, A. D., et al. (1997), PEACE: A Plasma Electron And Current Experiment, *Space Sci. Rev.*, *79*, 351.
- Karlsson, T., and G. Marklund (1998), Simulations of effects of small-scale auroral current closure in the return current region, *Phys. Space Plasmas*, *15*.
- Lysak, R. L., and Y. Song (2002), Energetics of the ionospheric feedback interaction, *J. Geophys. Res.*, *107*(A8), 1160, doi:10.1029/2001JA000308.
- Marklund, G., L. Blomberg, C.-G. Falthammar, and P. A. Lindqvist (1994), On intense diverging electric fields associated with black aurora, *Geophys. Res. Lett.*, *21*, 1859.
- Marklund, G. T., et al. (2001), Temporal evolution of the electric field accelerating electrons away from the auroral ionosphere, *Nature*, *414*, 724.
- Scofield, H. C., T. K. Yeoman, D. M. Wright, S. E. Milan, A. N. Wright, and R. J. Strangeway (2005), An investigation of the field aligned currents associated with a large scale ULF wave using data from CUTLASS and FAST, *Ann. Geophys.*, *23*, 487.
- Scofield, H. C., T. K. Yeoman, D. M. Wright, S. E. Milan, A. N. Wright, and R. J. Strangeway (2007), An investigation of the field aligned currents associated with a large scale ULF wave in the morning sector, *Planet. Space Sci.*, *55*, 770.
- Streltsov, A. V. (2007), Narrowing of the discrete auroral arc by the ionosphere, *J. Geophys. Res.*, *112*, A10218, doi:10.1029/2007JA012402.
- Streltsov, A. V., and W. Lotko (2004), Multiscale electrodynamics of the magnetosphere-ionosphere system, *J. Geophys. Res.*, *109*, A09214, doi:10.1029/2004JA010457.
- Streltsov, A. V., and W. Lotko (2005), Ultra-low-frequency electrodynamics of the magnetosphere–ionosphere interaction, *J. Geophys. Res.*, *110*, A08203, doi:10.1029/2004JA010764.
- Streltsov, A., and G. T. Marklund (2006), Divergent electric fields in downward current channels, *J. Geophys. Res.*, *111*, A07204, doi:10.1029/2005JA011196.
- Temerin, M., and C. W. Carlson (1998), Current-voltage relationship in the downward auroral current region, *Geophys. Res. Lett.*, *25*, 2365.
- Torkar, K., K. R. Svnes, A. Fazakerley, S. Szita, H. Rme, I. Dandouras, M. Fehringer, C. P. Escoubet, and M. Andr (2005), Improvement of plasma measurements onboard Cluster due to spacecraft potential control, *Adv. Space Res.*, *36*, 1951–1957.
- Tsyganenko, N. A. (1995), Modeling the Earth's magnetospheric magnetic field confined within a realistic magnetopause, *J. Geophys. Res.*, *100*, 5599.

C. C. Chaston, Space Sciences Laboratory, University of California, 7 Gauss Way, Berkeley, CA 94720-7450, USA.

M. W. Dunlop, CCLRC Rutherford Appleton Laboratory, Chilton, Didcot, Oxfordshire OX11 0QX, UK.

C. J. Owen, University College London, Mullard Space Science Laboratory, Holmbury St. Mary, Dorking, Surrey RH5 6NT, UK.

A. N. Wright, Mathematical Institute, University of St. Andrews, North Haugh, St. Andrews, Fife KY16 9SS, Scotland. (andy@mcs.st-and.ac.uk)